

Task-Specific Normalization for Continual Learning of Blind Image Quality Models

Weixia Zhang, *Member, IEEE*, Kede Ma, *Member, IEEE*, Guangtao Zhai, *Senior Member, IEEE*, and Xiaokang Yang, *Fellow, IEEE*

Abstract—The computational vision community has recently paid attention to continual learning for blind image quality assessment (BIQA). The primary challenge is to combat *catastrophic forgetting* of previously-seen IQA datasets (*i.e.*, tasks). In this paper, we present a simple yet effective continual learning method for BIQA with improved quality prediction accuracy, plasticity-stability trade-off, and task-order/length robustness. The key step in our approach is to freeze all convolution filters of a pre-trained deep neural network (DNN) for an explicit promise of stability, and learn task-specific normalization parameters for plasticity. We assign each new task a prediction head, and load the corresponding normalization parameters to produce a quality score. The final quality estimate is computed by feature fusion and adaptive weighting using hierarchical representations, without leveraging the test-time oracle. Extensive experiments on six IQA datasets demonstrate the advantages of the proposed method in comparison to previous training techniques for BIQA.

Index Terms—Blind image quality assessment, continual learning, task-specific normalization.

I. INTRODUCTION

THERE is an emerging trend to develop image quality assessment (IQA) models [1] and image processing methods in an alternating manner: better IQA models provide more reliable guidance to the design and optimization of the latter, while new image processing algorithms call for the former to handle unseen visual artifacts. This suggests a desirable IQA model to easily adapt to novel distortions by continually learning from new data (see Fig. 1).

This paper focuses on continual learning of blind IQA (BIQA) models [2], [3], which predict the perceptual quality of a “distorted” image without reference to an original undistorted image. Over the past 20 years, the research in BIQA has shifted from handling distortion-specific [4], single-stage [5], synthetic artifacts to general-purpose [6], multi-stage [7], authentic ones, and from relying on hand-engineered features to purely data-driven approaches [8]. Existing BIQA models are generally developed and tested using human-rated images from the same dataset, *i.e.*, within the same subpopulation [2]. As such, even the best-performing BIQA methods, *e.g.*, those

This work was supported in part by the National Natural Science Foundation of China under Grants 62071407 and 61901262, the RGC Early Career Scheme (No. 9048212), and the CityU Strategic Research Grant (No. 7005560).

Weixia Zhang, Guangtao Zhai, and Xiaokang Yang are with the MoE Key Lab of Artificial Intelligence, AI Institute, Shanghai Jiao Tong University, Shanghai, China (e-mail: zwx8981@sjtu.edu.cn; zhaiguangtao@sjtu.edu.cn; xkyang@sjtu.edu.cn).

Kede Ma is with the Department of Computer Science, City University of Hong Kong, Kowloon, Hong Kong (e-mail: kede.ma@cityu.edu.hk).

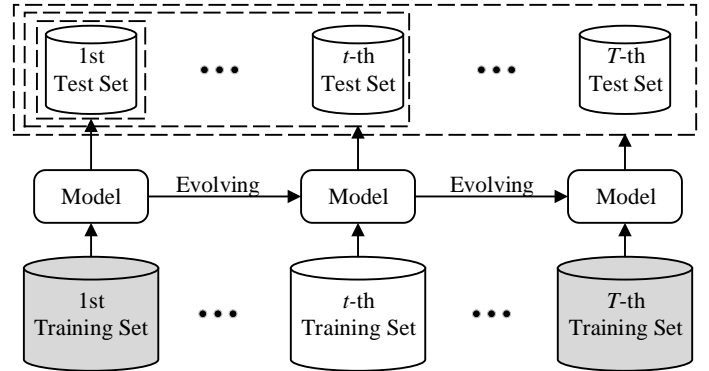


Fig. 1. Illustration of continual learning for BIQA. The grey cylinders denote the inaccessibility of previous and future training data. During testing, we use all previous and the current test sets to evaluate the stability and plasticity of the learned BIQA model, respectively.

based on deep neural networks (DNNs) are bound to encounter subpopulation shift when deployed in the real world.

Direct fine-tuning model parameters with new data may result in *catastrophic forgetting* [9], [10] of previously-seen data. The dataset combination trick in [11] has been proven effective in handling subpopulation shift, but is limited by the computational scalability and the dataset accessibility. Recently, Zhang *et al.* [2] formulated continual learning for BIQA with five desiderata. Meanwhile, they described the first continual learning method of training BIQA models based on a technique called learning with forgetting (LwF) [12]. Like many continual learning methods (for classification), LwF adds a form of regularization [13] to mildly adjust model parameters for new tasks while respecting old tasks. Nevertheless, this type of regularization-based methods have two limitations. First, it is practically difficult to set the trade-off parameter for the stability (*i.e.*, the ability to consolidate acquired knowledge from old tasks) and the plasticity (*i.e.*, the ability to learn new knowledge from the current task). Second, the performance is usually sensitive to the order and the length of the task sequence [2], [14].

In this paper, we describe a simple yet effective continual learning method for BIQA based on parameter decomposition. Specifically, we start with a pre-trained DNN for object recognition [15] as the multi-stage feature extractor due to its transferable feature hierarchies [16]. We freeze all convolution filters, and share them across tasks during the entire continual learning process. We append a prediction head, implemented by a fully connected layer, when learning a new task. We allow

the parameters of batch normalization (BN) [17] following each convolution to be specifically learned for each task. Through this *task-specific* normalization, a better plasticity-stability trade-off can be made with a negligible increase in model size. During inference, we load each group of BN parameters to produce a quality estimate using the corresponding prediction head. The final quality score is computed by feature fusion and adaptive weighting [2] based on hierarchical representations.

In summary, our contributions are threefold.

- We propose the task-specific normalization to improve continual learning for BIQA, where new knowledge can be integrated into BN parameters without catastrophic forgetting of acquired knowledge.
- We enhance the feature fusion and adaptive weighting modules with hierarchical feature representations, which is enabled by the proposed parameter decomposition scheme.
- We perform extensive experiments to demonstrate the advantages of our method in terms of quality prediction accuracy, plasticity-stability trade-off, and task-order/length robustness.

The remaining paper is organized as follows. Section II discusses the related work, putting our method in a proper context. Section III describes the proposed continual learning method with emphasis on the task-specific normalization. Section IV presents the experimental results, comparing the proposed method against existing training strategies. We conclude with a discussion in Section V.

II. RELATED WORK

In this section, we give an overview of recent progress in BIQA, especially on handling subpopulation shift. We then review representative continual learning methods for classification, and discuss normalization techniques in deep learning.

A. BIQA Models

Many early BIQA methods are based on hand-engineered natural scene statistics (NSS) in spatial [6], [18], transformed [19], or both domains [20]. In recent years, deep learning began to show its promise in the field of BIQA. Patchwise training [8], [21], transfer learning [22], and quality-aware pre-training [23]–[25] were proposed to compensate for the lack of human-rated data. Of particular interest is the introduction of IQA datasets with realistic distortions [26]–[28], which excites a series of BIQA models to address the synthetic-to-real generalization. Zhang *et al.* [29] assembled two network branches to account for synthetic and realistic distortions separately. Su *et al.* [30] investigated content-aware convolution for robust BIQA, while Zhu *et al.* [31] aimed to learn more transferable quality-aware representations by meta-learning. Zhang *et al.* [11] proposed a dataset combination strategy to train BIQA models on multiple IQA datasets. They later introduced a continual learning method for BIQA by combining LwF [12] with adaptive weighting [2]. Concurrently, Liu *et al.* [3] proposed a continual learning method

for BIQA based on a replay strategy. In this paper, we aim to accomplish something in the same spirit, proposing a continual learning method for BIQA with significantly improved performance in several aspects.

B. Continual Learning for Classification

While humans rarely forget previously-learned knowledge catastrophically, machine learning models such as DNNs tend to completely forget old concepts when learning new ones [10], [32]. Enforcing regularization is a common practice to mitigate the catastrophic forgetting problem in continual learning. For example, Li and Hoiem [12] proposed LwF, which leverages model predictions of previous tasks as pseudo labels. Elastic weight consolidation (EWC) [33], variational continual learning (VCL) [34], synaptic intelligence (SI) [35], and memory-aware synapses (MAS) [36] work similarly by identifying and penalizing changes to important parameters of previous tasks. From this perspective, parameter decomposition [13] can be seen as a form of hard regularization, disentangling model parameters into generic and task-specific groups. This may be done by either masking learned parameters of previous tasks [37]–[39] or growing new branches to accommodate new tasks [40]. For example, Yoon *et al.* [14] proposed additive parameter decomposition to achieve task-order robustness. Singh *et al.* [41] calibrated the convolution responses of a continually trained DNN with a few parameters for new tasks. In this paper, we take a similar but much simpler parameter decomposition approach to achieve accurate and robust continual learning for BIQA. More importantly, our method does not rely on the task oracle during inference, which is in stark contrast to continual learning methods for classification.

C. Normalization in Deep Learning

There is increasing evidence that normalization is a canonical neural computation throughout the visual system, and in many other sensory modalities and brain regions [42]. As biologically inspired, deep learning also incorporates different instantiations of normalization for various purposes, such as accelerating model training [17] and improving model generalization [43]. BN is a *de facto* technique to improve the training efficiency of DNNs, in which the convolution responses are divided by the standard deviation (std) of a pool of responses along the batch (and spatial) dimensions. Xie *et al.* [44] learned separate BN layers to harness adversarial examples, which improves image recognition models. Li *et al.* [45] proposed adaptive BN for domain adaptation, assuming that domain-invariant and domain-specific computations are learned by the convolution filters and the BN layers, respectively. Chang *et al.* [46] specialized BN layers using a two-stage algorithm for unsupervised domain adaptation. Dumoulin *et al.* [47] relied on conditional instance normalization [48] to synthesize the artistic styles of diverse paintings. Zhang *et al.* [49] presented a passport normalization for deep model intellectual property protection against infringement threats. In this paper, we introduce task-specific BN to accomplish continual learning of DNN-based BIQA models.

III. PROPOSED METHOD

In this section, we first revisit the formulation of continual learning for BIQA in [2]. We then elaborate the training and inference procedures of the proposed method.

A. Problem Formulation

When training on the t -th dataset \mathcal{D}_t , *i.e.*, the t -th task, a BIQA model f_w , parameterized by a vector w , has no direct access to previous training images in $\{\mathcal{D}_k\}_{k=1}^{t-1}$, leading to the following objective:

$$\mathcal{L}(\mathcal{D}_t; w) = \frac{1}{|\mathcal{D}_t|} \sum_{(x,q) \in \mathcal{D}_t} \ell(f_w(x), q) + \lambda r(w), \quad (1)$$

where x and q denote the ‘‘distorted’’ image and the corresponding mean opinion score (MOS), respectively. $\ell(\cdot)$ is a quantitative measure of quality prediction performance, and $r(\cdot)$ is an optional regularizer. A good BIQA model under this setting should adapt well to new tasks, and meanwhile endeavor to mitigate catastrophic forgetting of old tasks as measured by

$$\sum_{k=1}^t \mathcal{L}(\mathcal{V}_k; w) = \sum_{k=1}^t \left(\frac{1}{|\mathcal{V}_k|} \sum_{(x,q) \in \mathcal{V}_k} \ell(f_w(x), q) \right), \quad (2)$$

where \mathcal{V}_k denotes the test set for the k -th task. Five desiderata are suggested in [2] to make continual learning for BIQA feasible and nontrivial, which we briefly summarize as follows.

- I Common Perceptual Scale.** There exists a *monotonic* function for each of the IQA datasets to map their MOSs to a common perceptual scale. Otherwise, learning a single f_w on multiple IQA datasets (continually) is conceptually infeasible. This would require that MOSs of different datasets are collected under similar viewing conditions. Of course, Desideratum I also excludes human-rated datasets, recording perceptual quantities that are closely related to, but not image quality.
- II Apparent Subpopulation Shift.** At least two datasets in a task sequence should exhibit apparent subpopulation shift. This is to make continual learning for BIQA nontrivial because existing models show reasonable generalization to test images with similar distortion appearances (*i.e.*, mild subpopulation shift).
- III No Direct Access to Previous Data.** Despite the fact that continual learning methods for classification [13] may use the replay trick to combat catastrophic forgetting [50]. In the context of BIQA, Zhang *et al.* [2] assumed no direct access to previous data when learning new tasks. Notwithstanding, Desideratum III permits summarizing datasets with negligible bits of statistics. In this paper, we choose to respect this desideratum for a fair performance comparison.
- IV No Test-Time Oracle.** During inference, BIQA methods are unaware of which dataset the test image belongs to. Similar as Desideratum II, this is imperative, otherwise it would be trivial to train a separate model for each dataset.
- V Bounded Model Size.** The number of learnable parameters introduced by a new task should be negligible

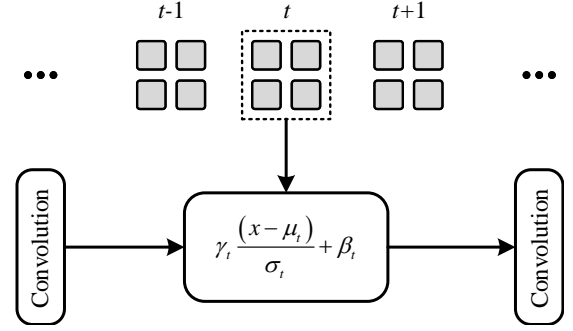


Fig. 2. Illustration of task-specific BN. The parameters of all convolutions are frozen and shared across all tasks. A group of BN parameters is customized for each task.

compared to that of the current model, forcing model capacity to be allocated wisely.

B. Model Estimation

Inspired by UNIQUE [11], we exploit relative quality information to learn a common perceptual scale for all tasks. Specifically, given an image pair (x, y) , we compute a binary label:

$$r(x, y) = \begin{cases} 1 & \text{if } \mu_x \geq \mu_y \\ 0 & \text{otherwise} \end{cases}, \quad (3)$$

where μ_x and μ_y are the MOSs of x and y , respectively. Careful readers may find that we do not infer a continuous value $p(x, y)$, which denotes the probability of x perceived better than y based on the Thurstone’s model [51] or the Bradley-Terry model [52] as typically done in previous work [11], [25]. This is because the computed probability may vary with the precision of the subjective testing methodology. For example, if x is marginally better than y and a precise subjective method such as the two-alternative forced choice (2AFC) is adopted, $p(x, y)$ can be close to one. By contrast, if a less precise subjective method such as the single stimulus continuous quality rating is used, $p(x, y)$ may only be slightly larger than 0.5. Compared to $p(x, y)$, we also empirically observe that $r(x, y)$ leads to faster convergence and improved accuracy results. In summary, when learning the t -th task, we transform $\mathcal{D}_t = \{x_t^{(i)}, \mu_t^{(i)}\}_{i=1}^{|\mathcal{D}_t|}$ to $\mathcal{P}_t = \{(x_t^{(i)}, y_t^{(i)}), r_t^{(i)}\}_{i=1}^{N_t}$, where $N_t \leq \binom{|\mathcal{D}_t|}{2}$.

Our BIQA model consists of a hierarchical feature extractor implemented by a multi-stage DNN, $f_\phi(\cdot)$, producing a fixed-length image representation independent of input resolution. For the t -th task, we append a prediction head implemented by a fully connected layer, $h_{\psi_t}(\cdot)$, outputting a corresponding quality score. Under the Thurstone’s Case V model [51], we estimate the probability that x is of higher quality than y by

$$\hat{p}_t(x, y) = \Phi \left(\frac{h_{\psi_t}(f_\phi(x)) - h_{\psi_t}(f_\phi(y))}{\sqrt{2}} \right), \quad (4)$$

where the quality prediction variance is fixed to one. We measure the statistical distance between the ground-truth labels and predicted probabilities using the fidelity loss [53] due to

its favorable optimization behaviors [11]:

$$\ell(x, y; \phi, \psi_t) = 1 - \frac{\sqrt{r(x, y)\hat{p}_t(x, y)}}{\sqrt{(1-r(x, y))(1-\hat{p}_t(x, y))}}. \quad (5)$$

To make a better trade-off between plasticity and stability while keeping a bounded model size, our BIQA method chooses to maximally share computation across tasks, and customize a tiny fraction of parameters to account for the incremental difference introduced by new tasks. In particular, our feature extractor is composed of several stages of convolution, BN, halfwave-rectification (*i.e.*, ReLU nonlinearity), and max-pooling, followed by hierarchical feature fusion. We freeze all pre-trained convolution parameters during model development, and learn a group of 4-tuple BN parameters for the t -th task

$$z_{\text{BN}} = \gamma_t \left(\frac{z - \mu_t}{\sigma_t} \right) + \beta_t, \quad (6)$$

where μ_t and σ_t are the mean and the std estimated by exponentially weighted moving average over mini-batches. γ_t and β_t are the learnable scale and shift parameters (see also Fig. 2). After training on a T -length task sequence, we obtain T groups of task-specific BN parameters. To enhance feature expressiveness for quality prediction, we propose to fuse multi-stage features similar in [54]. We first select convolutions from S different stages, and append 1×1 convolution (with the same output channel), followed by global average pooling (GAP) and l_2 -normalization:

$$\tilde{f}_{\phi_s}(x) = \frac{\text{gap}(f_{\phi_s}(x))}{\|\text{gap}(f_{\phi_s}(x))\|_2}, \text{ for } s \in \{1, \dots, S\}, \quad (7)$$

where $f_{\phi_s}(x)$ is the responses of 1×1 convolution at the s -th stage. Empirically, feature projection onto the unit hypersphere is beneficial for the pursuit of a common perceptual scale and for the numerical stability. Last, we concatenate the l_2 -normalized features as the final image representation:

$$\tilde{f}_{\phi}(x) = \frac{1}{\sqrt{S}} \text{concat}(\tilde{f}_{\phi_1}(x), \dots, \tilde{f}_{\phi_S}(x)), \quad (8)$$

where the constant $\frac{1}{\sqrt{S}}$ is responsible for re-scaling the concatenated feature vector to the unit hypersphere.

C. Model Inference

During inference, we load the t -th group of parameters in BN, 1×1 convolution, and fully connected layers to compute the t -th quality score. Due to the unavailability of the task oracle, we propose to enhance the adaptive weighting in [2] with hierarchical feature representations. It is noteworthy that our enhancement is made possible within the proposed parameter decomposition scheme.

Since our DNN-based feature extractor f_{ϕ} is pre-trained for object recognition [15], where we keep all convolution filters intact, it is straightforward to retrieve the pre-trained BN parameters that are content-aware and task-agnostic for reliable weight computation. We present the overview of the inference process in Fig. 3. During learning the t -th task, we use the pre-trained f_{ϕ} to compute globally pooled convolution responses of image x at the s -th stage, $f_{\phi_s}(x)$. Given S -stage convolutions, we obtain a feature summary of \mathcal{D}_t :

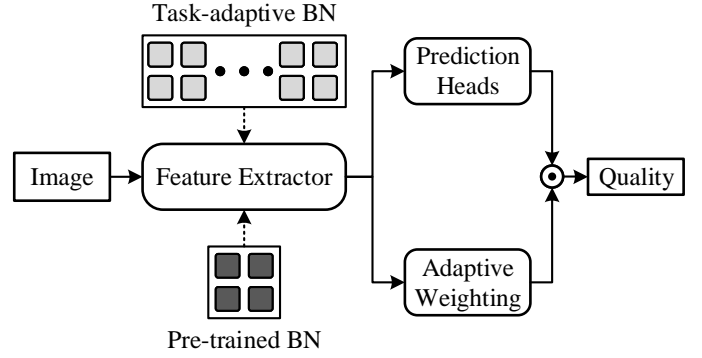


Fig. 3. Overview of the inference process. The dotted lines indicate loading the corresponding BN parameters.

$\{\tilde{f}_{\phi_1}(x_t^{(i)}), \dots, \tilde{f}_{\phi_S}(x_t^{(i)})\}_{i=1}^{|\mathcal{D}_t|}$. We then apply K -means [55] (for each stage of convolution responses) to compute S groups of K centroids $\{\{c_{kst}\}_{k=1}^K\}_{s=1}^S$.

We measure the perceptual relevance of the test image x to \mathcal{D}_t by computing the minimal Euclidean distances between $\tilde{f}_{\phi_s}(x)$ and $\{c_{kst}\}_{k=1}^K$:

$$d_{st}(x) = \min_k \|\tilde{f}_{\phi_s}(x) - c_{kst}\|_2. \quad (9)$$

We pass $\{d_{st}(x)\}_{t=1}^T$ to a softmax function to compute the adaptive weighting at the s -th stage for the t -th prediction head:

$$a_{st}(x) = \frac{\exp(-\tau d_{st}(x))}{\sum_{t=1}^T \exp(-\tau d_{st}(x))}, \quad (10)$$

where $\tau \geq 0$ is a parameter to control the smoothness of the softmax function. We further average the adaptive weightings across stages to obtain

$$a_t(x) = \frac{1}{S} \sum_s a_{st}(x). \quad (11)$$

We last compute the overall quality score by the inner product between the adaptive weighting and quality prediction vectors:

$$\hat{q}(x) = \sum_{t=1}^T a_t(x) h_{\psi_t}(f_{\phi}(x)). \quad (12)$$

IV. EXPERIMENTS

In this section, we first describe the experimental setup for continual learning of BIQA models, and then compare the proposed method against previous training techniques, supplemented by abundant ablation studies. The source code will be made publicly available at <https://github.com/zwx8981> to facilitate reproducible research.

A. Experimental Setup

We select six widely used IQA datasets: LIVE [5], CSIQ [56], BID [26], LIVE Challenge [27], KonIQ-10K [28], and KADID-10K [57]. We summarize the details of the six datasets in Table I. In general, the number of training pairs is proportional to the number of images in the training set of each dataset. As previously discussed, the diversity of

TABLE I

SUMMARY OF IQA DATASETS USED IN OUR EXPERIMENTS. CLIVE STANDS FOR THE LIVE CHALLENGE DATABASE. SS: SINGLE STIMULUS. DS: DOUBLE STIMULUS. MS: MULTIPLE STIMULUS. CQR: CONTINUOUS QUALITY RATING. ACR: ABSOLUTE CATEGORY RATING. CS: CROWDSOURCING

Dataset	# of Images	# of Training Pairs	# of Test Images	Scenario	# of Types	Testing Methodology	Year
LIVE [5]	779	7,780	163	Synthetic	5	SS-CQR	2006
CSIQ [56]	866	8,786	173	Synthetic	6	MS-CQR	2010
BID [26]	586	11,204	117	Realistic	N.A.	SS-CQR	2011
CLIVE [27]	1,162	24,604	232	Realistic	N.A.	SS-CQR-CS	2016
KonIQ-10K [28]	10,073	139,274	2,015	Realistic	N.A.	SS-ACR-CS	2018
KADID-10K [57]	10,125	140,071	2,000	Synthetic	25	DS-ACR-CS	2019

TABLE II

PERFORMANCE COMPARISON IN TERMS OF MPSR AND WEIGHTED SRCC, WHERE THE WEIGHTING IS PROPORTIONAL TO THE SIZE OF THE TEST SET. TASK-AWARE AND TASK-AGNOSTIC EVALUATION SETTINGS CORRESPOND TO QUALITY PREDICTION WITH AND WITHOUT THE TASK ORACLE, RESPECTIVELY. ALL METHODS ARE TRAINED IN CHRONOLOGICAL ORDER. BEST RESULTS IN THE SECOND SECTION ARE HIGHLIGHTED IN BOLD

Setting	Method	MPSR	Weighted SRCC
Task-aware	LwF-O	0.819	0.833
	SI-O	0.829	0.802
	MAS-O	0.814	0.790
	Proposed-O	0.860	0.855
Task-agnostic	SL	0.679	0.707
	LwF	0.771	0.701
	LwF-AW	0.810	0.781
	SI	0.773	0.682
	SI-AW	0.801	0.759
	MAS	0.755	0.658
	MAS-AW	0.793	0.762
	Proposed	0.839	0.798

subjective testing methodologies among different datasets may result in varying MOS precision [58], [59], encouraging us to consider binary ground-truth labels in Eq. (3). Following [2], we organize these datasets in chronological order for the main experiments. We randomly sample 80% images from each dataset for training, and leave the remaining for testing. To ensure content independence in LIVE, CSIQ, and KADID-10K, we divide the training and test sets according to the reference images.

We choose a variant of ResNet-18 [60] as the feature extractor. We keep the front convolution and four residual blocks, which are indexed by Stage 1 to Stage 4, respectively. We form hierarchical image representation (see Eq. (8)) and compute adaptive weightings (see Eq. (9)) using the convolution responses from Stages 2, 3 and 4. The output channel for 1×1 convolution is set to 64, which determines the channels of the fully connected layers for quality prediction to be 192×1 . As such, 64,480 parameters which account for about 0.64% of the total parameters are introduced for each new task, conforming to the bounded model size desideratum.

For each task, stochastic optimization is carried out by Adam [61] with an initial learning rate of 1×10^{-3} . We decay the learning rate by a factor of 10 at the sixth epoch, and train

our method for a maximum of seven epochs. During testing, the number of centroids used in K -means is set to $K = 128$ for all tasks. Empirically, we find that the performance is insensitive to the choice of K . We set the temperature to $\tau = 64$ in Eq. (10). We test on images of original size.

We use the Spearman’s rank correlation coefficient (SRCC) to measure the prediction performance. We evaluate the plasticity-stability ratio of a BIQA method by

$$\text{MPSR} = \frac{1}{T} \sum_{t=1}^T \text{PSR}_t \quad (13)$$

and

$$\text{PSR}_t = \begin{cases} \text{SRCC}_t & t = 1 \\ \left(\frac{1}{t-1} \sum_{k=1}^{t-1} \frac{\text{SRCC}_{tk}}{\text{SRCC}_k} \right) \cdot \text{SRCC}_t & t > 1, \end{cases} \quad (14)$$

where SRCC_{tk} , for $k \leq t$, is the SRCC result of the model on the k -th test set when it has just learned on the t -th dataset.

B. Competing Methods

We describe several competing methods for training.

- **Separate Learning (SL)** is the standard in BIQA, which trains the model using a single prediction head on one of the six training sets.
- **Joint Learning (JL)** is a recently proposed dataset combination trick [11] to address the cross-distortion-scenario challenge in BIQA. As an upper bound of all continual learning methods, JL trains the model with a single head on the combination of all six training sets.
- **LwF [12]** in BIQA is based on a multi-head architecture, which introduces a stability regularizer that uses the previous model outputs as soft labels to to preserve the performance of previously-seen data. LwF relies on the newest head for quality prediction. We also leverage the task oracle to select the corresponding head for quality prediction, denoted by **LwF-O**.
- **LwF-AW [2]**¹ is the first continual learning method for BIQA, which can be seen as the combination of LwF and vanilla adaptive weighting.
- **SI [35]** is also a regularization-based continual learning method, which estimates important parameters for previous tasks. When learning the t -th task, SI maintains an

¹Our implementation slightly differs from that provided by the original authors [2] in that we use binary labels instead of probabilities.

TABLE III
PERFORMANCE COMPARISON IN TERMS OF SRCC BETWEEN THE PROPOSED METHOD AND OTHERS. BEST RESULTS IN EACH SECTION ARE HIGHLIGHTED IN BOLD, AND RESULTS OF FUTURE TASKS ARE MARKED IN GREY

Dataset	Method	LIVE [5]	CSIQ [56]	BID [26]	CLIVE [27]	KonIQ-10K [28]	KADID-10K [57]
All	JL	0.969	0.815	0.842	0.827	0.856	0.896
LIVE	SL	0.968	0.653	0.719	0.446	0.634	0.509
	LwF	0.927	0.572	0.653	0.480	0.723	0.567
	LwF-AW	0.927	0.572	0.653	0.480	0.723	0.567
	SI	0.927	0.572	0.653	0.480	0.723	0.567
	SI-AW	0.927	0.572	0.653	0.480	0.723	0.567
	MAS	0.927	0.572	0.653	0.480	0.723	0.567
	MAS-AW	0.927	0.572	0.653	0.480	0.723	0.567
	Proposed	0.958	0.677	0.645	0.465	0.680	0.504
CSIQ	SL	0.954	0.871	0.644	0.401	0.598	0.513
	LwF	0.947	0.818	0.709	0.526	0.760	0.609
	LwF-AW	0.906	0.781	0.703	0.546	0.755	0.549
	SI	0.943	0.810	0.709	0.512	0.748	0.613
	SI-AW	0.936	0.809	0.713	0.517	0.751	0.618
	MAS	0.940	0.809	0.705	0.510	0.746	0.612
	MAS-AW	0.935	0.806	0.708	0.516	0.750	0.618
	Proposed	0.959	0.851	0.672	0.477	0.696	0.522
BID	SL	0.448	0.395	0.812	0.735	0.675	0.258
	LwF	0.818	0.866	0.791	0.704	0.737	0.394
	LwF-AW	0.935	0.787	0.792	0.672	0.741	0.470
	SI	0.846	0.741	0.803	0.721	0.745	0.480
	SI-AW	0.883	0.760	0.804	0.712	0.751	0.491
	MAS	0.815	0.705	0.802	0.728	0.741	0.455
	MAS-AW	0.857	0.729	0.803	0.719	0.748	0.470
	Proposed	0.963	0.889	0.818	0.720	0.701	0.494
CLIVE	SL	0.485	0.443	0.831	0.852	0.742	0.322
	LwF	0.766	0.638	0.830	0.852	0.763	0.425
	LwF-AW	0.920	0.778	0.800	0.818	0.779	0.544
	SI	0.818	0.698	0.832	0.851	0.762	0.456
	SI-AW	0.843	0.706	0.829	0.847	0.770	0.463
	MAS	0.769	0.674	0.828	0.848	0.766	0.495
	MAS-AW	0.784	0.694	0.827	0.844	0.774	0.479
	Proposed	0.960	0.847	0.840	0.847	0.730	0.502
KonIQ-10K	SL	0.640	0.600	0.775	0.745	0.850	0.534
	LwF	0.763	0.678	0.750	0.735	0.872	0.540
	LwF-AW	0.929	0.794	0.782	0.791	0.848	0.580
	SI	0.749	0.711	0.761	0.714	0.857	0.524
	SI-AW	0.909	0.796	0.802	0.772	0.842	0.551
	MAS	0.713	0.702	0.753	0.703	0.859	0.525
	MAS-AW	0.879	0.803	0.792	0.767	0.850	0.557
	Proposed	0.961	0.766	0.826	0.835	0.845	0.568
KADID-10K	SL	0.931	0.718	0.606	0.468	0.611	0.817
	LwF	0.868	0.753	0.626	0.361	0.580	0.847
	LwF-AW	0.889	0.790	0.759	0.728	0.818	0.741
	SI	0.877	0.724	0.662	0.432	0.566	0.807
	SI-AW	0.873	0.865	0.830	0.761	0.782	0.712
	MAS	0.852	0.702	0.653	0.388	0.530	0.798
	MAS-AW	0.854	0.833	0.781	0.751	0.775	0.735
	Proposed	0.961	0.770	0.827	0.835	0.847	0.732

online estimate

$$w_t = \frac{\partial f_\phi(x)}{\partial \phi_t} \odot (\phi_t - \phi_{t-1}), \quad (15)$$

where $f_\phi(x)$ is the learned BIQA function, parameterized by the vector ϕ and \odot is the Hadamard product. ϕ_{t-1} records the values of the parameter vector before learning the t -th task. A cumulative importance measure is then

updated:

$$W_t = \sum_{i=1}^t \frac{w_i}{(\phi_i - \phi_{i-1})^2 + c}, \quad (16)$$

where ϕ_0 denotes the initial weights and c is a damping parameter to avoid any division by zero. Similar to LwF, we implement a multi-head architecture for SI, and rely on the newest head to predict image quality. We try to improve the performance with the adaptive weighting

TABLE IV

PERFORMANCE COMPARISON IN TERMS OF SRCC BETWEEN THE PROPOSED METHOD AND OTHERS WHEN THE TEST-TIME ORACLE IS AVAILABLE. BEST RESULTS IN EACH SECTION ARE HIGHLIGHTED IN BOLD

Dataset	Method	LIVE [5]	CSIQ [56]	BID [26]	CLIVE [27]	KonIQ-10K [28]	KADID-10K [57]
All	JL	0.969	0.815	0.842	0.827	0.856	0.896
LIVE	LwF-O	0.927	–	–	–	–	–
	SI-O	0.927	–	–	–	–	–
	MAS-O	0.927	–	–	–	–	–
	Proposed-O	0.958	–	–	–	–	–
CSIQ	LwF-O	0.876	0.818	–	–	–	–
	SI-O	0.941	0.810	–	–	–	–
	MAS-O	0.941	0.809	–	–	–	–
	Proposed-O	0.958	0.837	–	–	–	–
BID	LwF-O	0.918	0.790	0.791	–	–	–
	SI-O	0.905	0.769	0.803	–	–	–
	MAS-O	0.881	0.741	0.802	–	–	–
	Proposed-O	0.958	0.837	0.820	–	–	–
CLIVE	LwF-O	0.906	0.763	0.749	0.852	–	–
	SI-O	0.878	0.728	0.833	0.851	–	–
	MAS-O	0.812	0.721	0.830	0.848	–	–
	Proposed-O	0.958	0.837	0.820	0.839	–	–
KonIQ-10K	LwF-O	0.915	0.756	0.738	0.832	0.872	–
	SI-O	0.929	0.836	0.814	0.785	0.857	–
	MAS-O	0.903	0.844	0.805	0.781	0.859	–
	Proposed-O	0.958	0.837	0.820	0.839	0.849	–
KADID-10K	LwF-O	0.888	0.758	0.721	0.794	0.833	0.847
	SI-O	0.865	0.857	0.823	0.784	0.788	0.807
	MAS-O	0.846	0.825	0.751	0.755	0.782	0.798
	Proposed-O	0.958	0.837	0.820	0.839	0.849	0.858

mechanism, denoted by **SI-AW**, and leverage the task oracle as well, denoted by **SI-O**.

- **MAS** [35] shares a similar philosophy with SI to penalize the changes to important weights. The difference lies in the calculation of the cumulative importance measure.

$$W_t = \sum_{i=1}^t \frac{1}{|\mathcal{D}_i|} \sum_{x \in \mathcal{D}_i} \left\| \frac{\partial f_\phi(x)}{\partial \phi_i} \right\|_2, \quad (17)$$

Similarly, MAS uses the latest head for quality prediction, and has two variants that include the adaptive weighting module and the task oracle, denoted by **MAS-AW** and **MAS-O**, respectively.

- The **proposed** method makes use of task-specific BN to handle new tasks, and enhances the adaptive weighting in [2] using rich feature hierarchies. We also replace the enhanced adaptive weighting with the task oracle for quality prediction, denoted by **Proposed-O**.

C. Main Results

Table II lists MPSR and weighted SRCC results on the six IQA test sets, where the weighting is proportional to the size of the test set (see Table I). Several interesting observations have been made. First, without any remedy for catastrophic forgetting, the performance of SL is far from satisfactory, consistent with previous findings [2]. Particularly, we identify a significant performance drop when SL transits from CSIQ to BID, where an apparent subpopulation shift from synthetic to realistic distortions is introduced. Second, direct application of LwF, SI, and MAS from image classification to BIQA

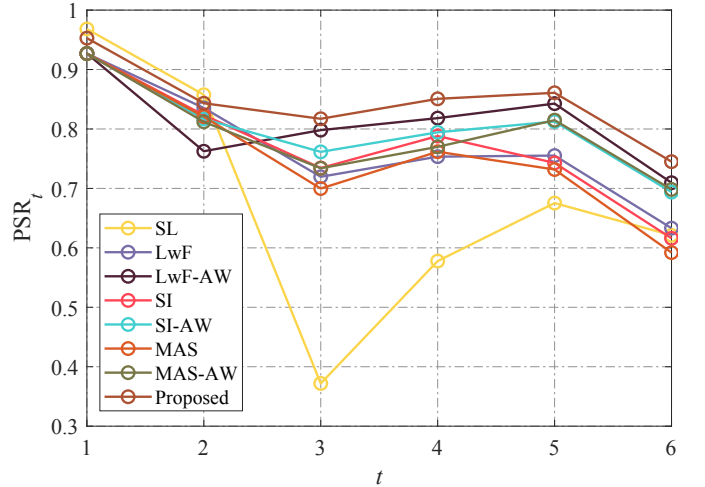


Fig. 4. PSR_t as a function of the task index t .

achieves better performance over SL in terms of MPSR, showing their effectiveness to balance between plasticity and stability. Nevertheless, their quality prediction performance in weighted SRCC is slightly worse than SL. Third, equipped with vanilla adaptive weighting, LwF-AW, SI-AW, and MAS-AW significantly outperform their counterparts under both measures. The performance is even comparable to their “upper bounds” (*i.e.*, LwF-O, SI-O, and MAS-O) in terms of MPSR. Fourth, the proposed method achieves the best results, which outperforms LwF-O, SI-O, and MAS-O in terms of MPSR by large margins. Nonetheless, the performance gap between the

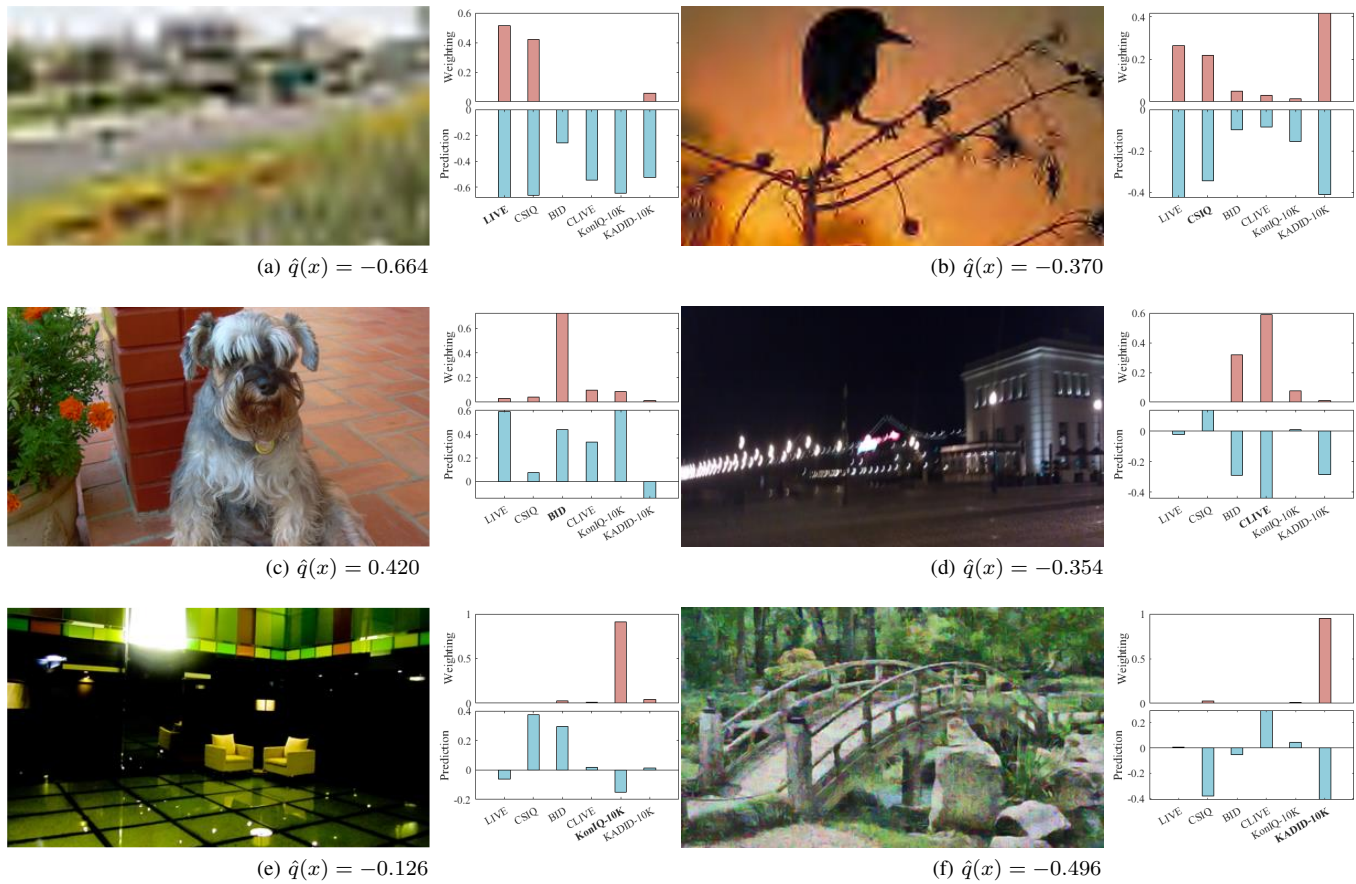


Fig. 5. Learned common perceptual scale to embed images from the six IQA datasets. The bar charts of adaptive weightings and quality predictions are also presented alongside each image. The dataset in bold indicates the origin of the test image. The final quality prediction $\hat{q}(x)$ is shown in the subcaption. Zoom in for better distortion visibility.

TABLE V

COMPARISON OF TASK-ORDER ROBUSTNESS MEASURED BY THE MEAN MPSR UNDER DIFFERENT TASK ORDERS. I: DEFAULT CHRONOLOGICAL ORDER. II: SYNTHETIC AND REALISTIC DISTORTIONS IN ALTERNATION. III: SYNTHETIC DISTORTIONS FOLLOWED BY REALISTIC DISTORTIONS. IV: REALISTIC DISTORTIONS FOLLOWED BY SYNTHETIC DISTORTIONS. V TO VIII: REVERSES OF ORDERS I TO IV, RESPECTIVELY

Order	LwF-AW	SI-AW	MAS-AW	Proposed
I	0.810	0.801	0.792	0.839
II	0.799	0.800	0.801	0.844
III	0.816	0.798	0.806	0.845
IV	0.794	0.802	0.809	0.831
V	0.811	0.778	0.791	0.808
VI	0.806	0.768	0.780	0.828
VII	0.788	0.766	0.785	0.831
VIII	0.817	0.793	0.779	0.820
Mean	0.805	0.789	0.793	0.831

proposed method and Proposed-O indicates room for further improvement.

We plot PSR_t as a function of the task index t in Fig. 4, from which we find that our method is more stable as the length of the task sequence grows. We then look closely at the performance variations along the task sequence, and

summarize the SRCC results continually in Tables III and IV, corresponding to task-agnostic and task-aware evaluations, respectively. Several useful findings are worth mentioning. First, JL provides an effective but unscalable solution to the subpopulation shift in BIQA, serving as the upper bound of all continual learning methods. Second, the plasticity of SL is superior, but the results suffer from significant oscillation due to subpopulation shift between synthetic and realistic distortions [11], [22], [29]. Third, the favorable performance of LwF-AW, SI-AW, and MAS-AW against LwF, SI, and MAS especially on old tasks validates vanilla adaptive weighting for summarizing quality predictions. Fourth, with access to the task oracle, Proposed-O achieves comparable performance to JL, which verifies the effectiveness of our task-specific BN. Finally, the proposed method is able to deliver better performance than Proposed-O on some of the old tasks, indicating interesting backward knowledge transfer phenomenon.

We last conduct a qualitative analysis of our BIQA model by showing representative test images from the task sequence in Fig. 5. We find that for frequently-seen distortion appearances (e.g., global blurring in (a)), all heads tend to make reasonable predictions, and more weightings are given to the corresponding head. Meanwhile, if one distortion type occurs in multiple datasets (e.g., JPEG2000 compression in (b)), the heads that have seen the distortion work well, while others do not.

TABLE VI
COMPARISON OF TASK-LENGTH ROBUSTNESS MEASURED BY THE MEAN MPSR RESULTS UNDER DIFFERENT TASK LENGTHS FOR DIFFERENT TASK ORDERS

Order	I		II		III		IV	
Length	LwF-AW	Proposed	LwF-AW	Proposed	LwF-AW	Proposed	LwF-AW	Proposed
1	0.927	0.958	0.927	0.958	0.927	0.958	0.797	0.820
2	0.845	0.905	0.853	0.887	0.845	0.905	0.818	0.841
3	0.829	0.883	0.828	0.889	0.818	0.859	0.824	0.842
4	0.826	0.873	0.824	0.875	0.815	0.853	0.837	0.871
5	0.830	0.863	0.796	0.849	0.810	0.850	0.825	0.850
6	0.810	0.839	0.799	0.844	0.816	0.845	0.794	0.831
Mean	0.844	0.887	0.838	0.884	0.838	0.878	0.816	0.843
Order	V		VI		VII		VIII	
Length	LwF-AW	Proposed	LwF-AW	Proposed	LwF-AW	Proposed	LwF-AW	Proposed
1	0.809	0.858	0.884	0.849	0.884	0.849	0.809	0.858
2	0.826	0.804	0.812	0.803	0.842	0.835	0.821	0.819
3	0.813	0.789	0.805	0.805	0.822	0.834	0.848	0.852
4	0.810	0.790	0.790	0.794	0.783	0.810	0.844	0.837
5	0.798	0.782	0.787	0.802	0.774	0.804	0.825	0.825
6	0.811	0.808	0.806	0.828	0.788	0.831	0.817	0.820
Mean	0.811	0.805	0.814	0.813	0.816	0.827	0.827	0.835

TABLE VII
PERFORMANCE COMPARISON OF THE PROPOSED METHOD WITH DIFFERENT DESIGN CHOICES. WE TRAIN A SINGLE GROUP OF GENERIC BN PARAMETERS TO SHOW THE NECESSITY OF TASK-SPECIFIC BN. WE ALSO EXAM HOW FEATURE HIERARCHY AFFECTS THE FEATURE FUSION AND ADAPTIVE WEIGHTING MODULES, AND SUBSEQUENTLY THE QUALITY PREDICTION PERFORMANCE. THE DEFAULT SETTING IS HIGHLIGHTED IN BOLD

Design Choice		MPSR	Weighted SRCC
LwF-AW (as reference)		0.810	0.781
Generic BN		0.774	0.679
Feature Hierarchy	Stage 4	0.780	0.785
	Stages 3+4	0.834	0.786
	Stages 2+3+4	0.839	0.798
	Stages 1+2+3+4	0.835	0.795

Fortunately, the enhanced adaptive weighting by hierarchical feature representations is able to underweight inaccurate heads. Moreover, the learned BIQA model successfully aligns images of synthetic and realistic distortions in a common perceptual scale, despite not exposed to pairs of images from different distortion scenarios.

D. Results of Task-Order/Length Robustness

In real-world applications, novel distortions may emerge in arbitrary order. As a result, a continual learning method for BIQA is expected to be robust to different task orders. In addition to (I) the default chronological order, we experiment with seven more task orders: (II) synthetic and realistic distortions in alternation: LIVE \rightarrow BID \rightarrow CSIQ \rightarrow LIVE Challenge \rightarrow KADID-10K \rightarrow KonIQ-10K, (III) synthetic distortions followed by realistic distortions: LIVE \rightarrow CSIQ \rightarrow KADID-10K \rightarrow BID \rightarrow LIVE Challenge \rightarrow KonIQ-10K,

(IV) realistic distortions followed by synthetic distortions: BID \rightarrow LIVE Challenge \rightarrow KonIQ-10K \rightarrow LIVE \rightarrow CSIQ \rightarrow KADID-10K, and (V)-(VIII) the reverses of Orders (I)-(IV). We quantify the task-order robustness of a learning method by the average MPSR of different orders. We compare our method to LwF-AW [2], SI-AW, and MAS-AW in Table V. The main observation is that our method is more robust than LwF-AW, SI-AW, and MAS-AW for seven out of eight task orders. The only exception is Order V, where we begin with KADID-10K [57], a synthetic dataset that is considered visually much harder than LIVE [5] and CSIQ [56], therefore posing a challenge for performance stabilization. Given a specific task order, we also measure the task-length robustness by the mean MPSR of different lengths, $\{\text{MPSR}_t\}_{t=1}^T$. We compare our method to LwF-AW [2] in Table VI². We find the task-length robustness to be dependent on the task order, and our method performs better or on par with LwF-AW across all task orders. Relatively inferior results are observed for Orders V and VI, where KADID-10K [57] is listed in the first and second place, respectively. Altogether, these promising results indicate that our method has great potentials for use in practical quality prediction scenarios.

E. Ablation Studies

In this subsection, we conduct additional ablation experiments to probe the performance variations of our method with alternative design choices. Note that all experiments are conducted using the default chronological order. First, to verify the necessity of the core design of our method - task-specific BN, we train a single group of generic BN parameters along the task sequence. During inference, we use the converged

²As the task-length robustness of SI-AW and MAS-AW is inferior to LwF-AW, we omit their results in Table VI for neat presentation.

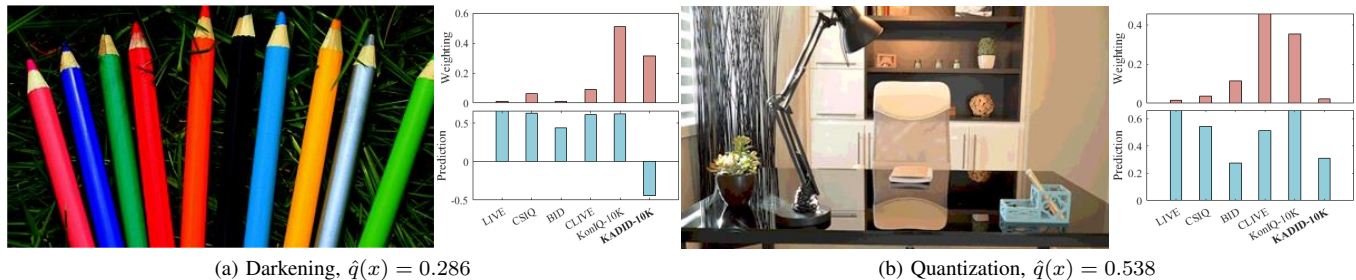


Fig. 6. Two failure cases of the adaptive weighting module in the proposed method. The two images are synthetically distorted by the darkening and quantization operations, respectively, in KADID-10K [57]. Our adaptive weighting module weights prediction heads for realistic distortions incorrectly high, leading to inaccurate quality predictions. Images are cropped for improved visibility.

BN parameters to make predictions for all tasks. As shown in Table VII, this attempt achieves an MPSR of 0.774 and a weighted SRCC of 0.679, which are far below the proposed method. We then evaluate the influence of the feature hierarchy on the feature fusion and the adaptive weighting modules by incorporating different stages of convolutions. The results in Table VII show that middle-stage features are more beneficial, and the combination of features across Stage 2 to Stage 4 delivers the most perceptual gains. These results provide solid justifications of the feature fusion and adaptive weighting modules enhanced by hierarchical representations.

F. Limitations

Although the proposed BIQA model in the continual learning setting achieves overall the best performance, it does not handle KADID-10k [57] satisfactorily. This can be observed by a sharp performance drop in the last row of Table III, indicating weak plasticity. Meanwhile, the relatively inferior MPSR results of Order V in Tables V and VI are largely caused by learning KADID-10K as the first task, indicating weak stability. We conjecture that this may be due to some difficult distortion types in KADID-10K, introducing challenging subpopulation shift to fail the adaptive weighting module as shown in Fig. 6. We are currently experimenting with different feature representations as inputs to our adaptive weighting module. Preliminary results show that representations that are more sensitive to synthetic distortions (*e.g.*, those from S-CNN in DB-CNN [29]) lead to more robust weighting with improved performance at the cost of additional model size expansion.

V. CONCLUSION AND DISCUSSION

We have introduced a simple yet effective method of continually learning BIQA models. The key to the success of our method is to train task-specific BN parameters for each task while holding all pre-trained convolution filters fixed. Along with hierarchical feature fusion and adaptive weighting, our method outperforms previous training methods in terms of quality prediction accuracy, plasticity-stability trade-off, and task-order/length robustness.

The current continual learning methods for BIQA rely on five desiderata as specified in [2], among which the assumption of a common perceptual scale is foremost. It

is well-known that the perceived quality of a visual image depends not only on the image content itself, but also on the subjective testing protocols as well as viewing conditions. For example, switching from single-stimulus methods to 2AFC approaches generally improves the accuracy of fine-grained quality annotations. We take this into consideration by pursuing binary labels as ground-truths. Moreover, the visibility of some distortions (*e.g.*, JPEG compression) varies with the equivalent viewing distance. Although it would be ideal to give a complete treatment of viewing conditions (*e.g.*, as part of model input), our computational study shows the possibility to learn a common perceptual scale for different IQA datasets with MOSs collected under similar viewing conditions and having overlapping quality ranges.

With the explosive growth of user-generated images, it is also desirable to perform online continual learning for BIQA, where there is no distinct boundaries between tasks (or datasets) during training. Under this setting, Desideratum III that requires no direct access to previous data seems too strict to satisfy. It remains to be seen whether this desideratum should be relaxed, allowing the widely practiced replay trick [50], [62], [63] in classification to be leveraged.

REFERENCES

- [1] Z. Wang and A. C. Bovik, *Modern Image Quality Assessment*. Morgan & Claypool, 2006.
- [2] W. Zhang, D. Li, C. Ma, G. Zhai, X. Yang, and K. Ma, “Continual learning for blind image quality assessment,” *CoRR*, vol. abs/2102.09717, 2021.
- [3] J. Liu, W. Zhou, J. Xu, X. Li, S. An, and Z. Chen, “LIQA: Lifelong blind image quality assessment,” *CoRR*, vol. abs/2104.14115, 2021.
- [4] Z. Wang, H. R. Sheikh, and A. C. Bovik, “No-reference perceptual quality assessment of JPEG compressed images,” in *IEEE International Conference on Image Processing*, vol. 1, 2002, pp. 477–480.
- [5] H. R. Sheikh, M. F. Sabir, and A. C. Bovik, “A statistical evaluation of recent full reference image quality assessment algorithms,” *IEEE Transactions on Image Processing*, vol. 15, no. 11, pp. 3440–3451, Nov. 2006.
- [6] A. Mittal, A. K. Moorthy, and A. C. Bovik, “No-reference image quality assessment in the spatial domain,” *IEEE Transactions on Image Processing*, vol. 21, no. 12, pp. 4695–4708, Dec. 2012.
- [7] D. Jayaraman, A. Mittal, A. K. Moorthy, and A. C. Bovik, “Objective quality assessment of multiply distorted images,” in *Signals, Systems and Computers*, 2013, pp. 1693–1697.
- [8] L. Kang, P. Ye, Y. Li, and D. Doermann, “Convolutional neural networks for no-reference image quality assessment,” in *IEEE Conference on Computer Vision and Pattern Recognition*, 2014, pp. 1733–1740.

- [9] J. L. McClelland, B. L. McNaughton, and R. C. O'Reilly, "Why there are complementary learning systems in the hippocampus and neocortex: Insights from the successes and failures of connectionist models of learning and memory," *Psychological Review*, vol. 102, no. 3, pp. 419–457, Jul. 1995.
- [10] M. McCloskey and N. J. Cohen, "Catastrophic interference in connectionist networks: The sequential learning problem," in *Psychology of Learning and Motivation*, 1989, pp. 109–165.
- [11] W. Zhang, K. Ma, G. Zhai, and X. Yang, "Uncertainty-aware blind image quality assessment in the laboratory and wild," *IEEE Transactions on Image Processing*, vol. 30, pp. 3474–3486, Mar. 2021.
- [12] Z. Li and D. Hoiem, "Learning without forgetting," *IEEE Transactions on Pattern Analysis and Machine Intelligence*, vol. 40, no. 12, pp. 2935–2947, Dec. 2018.
- [13] M. D. Lange, R. Aljundi, M. Masana, S. Parisot, X. Jia, A. Leonardis, G. Slabaugh, and T. Tuytelaars, "A continual learning survey: Defying forgetting in classification tasks," *IEEE Transactions on Pattern Analysis and Machine Intelligence*, to appear, 2021.
- [14] J. Yoon, S. Kim, E. Yang, and S. J. Hwang, "Scalable and order-robust continual learning with additive parameter decomposition," in *International Conference on Learning Representations*, 2020.
- [15] J. Deng, W. Dong, R. Socher, L.-J. Li, K. Li, and F.-F. Li, "ImageNet: A large-scale hierarchical image database," in *IEEE Conference on Computer Vision and Pattern Recognition*, 2009, pp. 248–255.
- [16] J. Yosinski, J. Clune, Y. Bengio, and H. Lipson, "How transferable are features in deep neural networks?" in *Advances in Neural Information Processing Systems*, vol. 2, 2014, pp. 3320–3328.
- [17] S. Ioffe and C. Szegedy, "Batch normalization: Accelerating deep network training by reducing internal covariate shift," in *International Conference on Machine Learning*, vol. 37, 2015, pp. 448–456.
- [18] A. Mittal, R. Soundararajan, and A. C. Bovik, "Making a "Completely Blind" image quality analyzer," *IEEE Signal Processing Letters*, vol. 20, no. 3, pp. 209–212, Mar. 2013.
- [19] A. K. Moorthy and A. C. Bovik, "Blind image quality assessment: From natural scene statistics to perceptual quality," *IEEE Transactions on Image Processing*, vol. 20, no. 12, pp. 3350–3364, Dec. 2011.
- [20] D. Ghadiyaram and A. C. Bovik, "Perceptual quality prediction on authentically distorted images using a bag of features approach," *Journal of Vision*, vol. 17, no. 1, pp. 32–59, Jan. 2017.
- [21] S. Bosse, D. Maniry, K. R. Müller, T. Wiegand, and W. Samek, "Deep neural networks for no-reference and full-reference image quality assessment," *IEEE Transactions on Image Processing*, vol. 27, no. 1, pp. 206–219, Jan. 2018.
- [22] H. Zeng, L. Zhang, and A. C. Bovik, "Blind image quality assessment with a probabilistic quality representation," in *IEEE International Conference on Image Processing*, 2018, pp. 609–613.
- [23] X. Liu, J. v. d. Weijer, and A. D. Bagdanov, "RankQA: Learning from rankings for no-reference image quality assessment," in *IEEE International Conference on Computer Vision*, 2017, pp. 1040–1049.
- [24] K. Ma, W. Liu, K. Zhang, Z. Duanmu, Z. Wang, and W. Zuo, "End-to-end blind image quality assessment using deep neural networks," *IEEE Transactions on Image Processing*, vol. 27, no. 3, pp. 1202–1213, Mar. 2018.
- [25] K. Ma, X. Liu, Y. Fang, and E. P. Simoncelli, "Blind image quality assessment by learning from multiple annotators," in *IEEE International Conference on Imaging Processing*, 2019, pp. 2344–2348.
- [26] A. Ciancio, A. L. N. T. Targino da Costa, E. A. B. da Silva, A. Said, R. Samadani, and P. Obrador, "No-reference blur assessment of digital pictures based on multifeature classifiers," *IEEE Transactions on Image Processing*, vol. 20, no. 1, pp. 64–75, Jan. 2011.
- [27] D. Ghadiyaram and A. C. Bovik, "Massive online crowdsourced study of subjective and objective picture quality," *IEEE Transactions on Image Processing*, vol. 25, no. 1, pp. 372–387, Jan. 2016.
- [28] V. Hosu, H. Lin, T. Sziranyi, and D. Saupe, "KonIQ-10k: An ecologically valid database for deep learning of blind image quality assessment," *IEEE Transactions on Image Processing*, vol. 29, pp. 4041–4056, Jan. 2020.
- [29] W. Zhang, K. Ma, J. Yan, D. Deng, and Z. Wang, "Blind image quality assessment using a deep bilinear convolutional neural network," *IEEE Transactions on Circuits and Systems for Video Technology*, vol. 30, no. 1, pp. 36–47, Jan. 2020.
- [30] S. Su, Q. Yan, Y. Zhu, C. Zhang, X. Ge, J. Sun, and Y. Zhang, "Blindly assess image quality in the wild guided by a self-adaptive hyper network," in *IEEE Conference on Computer Vision and Pattern Recognition*, 2020, pp. 3664–3673.
- [31] H. Zhu, L. Li, J. Wu, W. Dong, and G. Shi, "MetaIQA: Deep meta-learning for no-reference image quality assessment," in *IEEE Conference on Computer Vision and Pattern Recognition*, 2020, pp. 14 131–14 140.
- [32] R. M. French, "Catastrophic forgetting in connectionist networks," *Trends in Cognitive Sciences*, vol. 3, no. 4, pp. 128–135, Apr. 1999.
- [33] J. Kirkpatrick, R. Pascanu, N. Rabinowitz, J. Veness, G. Desjardins, A. A. Rusu, K. Milan, J. Quan, T. Ramalho, A. Grabska-Barwinska, C. Clopath, D. Kumaran, and R. Hadsell, "Overcoming catastrophic forgetting in neural networks," *National Academy of Sciences*, vol. 114, no. 13, pp. 3521–3526, Mar. 2017.
- [34] C. V. Nguyen, Y. Li, T. D. Bui, and R. E. Turner, "Variational continual learning," in *International Conference on Learning Representations*, 2018.
- [35] F. Zenke, B. Poole, and S. Ganguli, "Continual learning through synaptic intelligence," in *International Conference on Machine Learning*, vol. 70, 2017, pp. 3987–3995.
- [36] R. Aljundi, F. Babiloni, M. Elhoseiny, M. Rohrbach, and T. Tuytelaars, "Memory aware synapses: Learning what (not) to forget," in *European Conference on Computer Vision*, 2018, pp. 139–154.
- [37] C. Fernando, D. Banarse, C. Blundell, Y. Zwols, D. Ha, A. A. Rusu, A. Pritzel, and D. Wierstra, "PathNet: Evolution channels gradient descent in super neural networks," *CoRR*, vol. abs/1701.08734, 2017.
- [38] A. Mallya, D. Davis, and S. Lazebnik, "Piggyback: Adapting a single network to multiple tasks by learning to mask weights," in *European Conference on Computer Vision*, 2018, pp. 67–82.
- [39] A. Mallya and S. Lazebnik, "PackNet: Adding multiple tasks to a single network by iterative pruning," in *IEEE Conference on Computer Vision and Pattern Recognition*, 2018, pp. 7765–7773.
- [40] A. A. Rusu, N. C. Rabinowitz, G. Desjardins, H. Soyer, J. Kirkpatrick, K. Kavukcuoglu, R. Pascanu, and R. Hadsell, "Progressive neural networks," *CoRR*, vol. abs/1606.04671, 2016.
- [41] P. Singh, V. K. Verma, P. Mazumder, L. Carin, and P. Rai, "Calibrating CNNs for lifelong learning," in *Advances in Neural Information Processing Systems*, 2020, pp. 15 579–15 590.
- [42] M. Carandini and D. J. Heeger, "Normalization as a canonical neural computation," *Nature Reviews Neuroscience*, vol. 13, no. 1, pp. 51–62, Nov. 2012.
- [43] L. Huang, J. Qin, Y. Zhou, F. Zhu, L. Liu, and L. Shao, "Normalization techniques in training DNNs: Methodology, analysis and application," *CoRR*, vol. abs/2009.12836, 2020.
- [44] C. Xie, M. Tan, B. Gong, J. Wang, A. L. Yuille, and Q. V. Le, "Adversarial examples improve image recognition," in *IEEE Conference on Computer Vision and Pattern Recognition*, 2020, pp. 819–828.
- [45] Y. Li, N. Wang, J. Shi, J. Liu, and X. Hou, "Revisiting batch normalization for practical domain adaptation," in *IEEE International Conference on Learning Representations*, 2017.
- [46] W.-G. Chang, T. You, S. Seo, S. Kwak, and B. Han, "Domain-specific batch normalization for unsupervised domain adaptation," in *IEEE Conference on Computer Vision and Pattern Recognition*, 2019, pp. 7354–7362.
- [47] V. Dumoulin, J. Shlens, and M. Kudlur, "A learned representation for artistic style," in *International Conference on Learning Representations*, 2017.
- [48] D. Ulyanov, A. Vedaldi, and V. Lempitsky, "Instance normalization: The missing ingredient for fast stylization," *CoRR*, vol. abs/1607.08022, 2016.
- [49] J. Zhang, D. Chen, J. Liao, W. Zhang, G. Hua, and N. Yu, "Passport-aware normalization for deep model protection," in *Advances in Neural Information Processing Systems*, vol. 33, 2020, pp. 22 619–22 628.
- [50] S.-A. Rebuffi, A. Kolesnikov, G. Sperl, and C. H. Lampert, "iCaRL: Incremental classifier and representation learning," in *IEEE Conference on Computer Vision and Pattern Recognition*, 2017, pp. 2001–2010.
- [51] L. L. Thurstone, "A law of comparative judgment," *Psychological Review*, vol. 34, pp. 273–286, Jul. 1927.
- [52] B. Ralph A. and T. Milton E., "Rank analysis of incomplete block designs: I. The method of paired comparisons," *Biometrika*, vol. 39, pp. 324–345, Dec. 1952.
- [53] M.-F. Tsai, T.-Y. Liu, T. Qin, H.-H. Chen, and W.-Y. Ma, "FRank: A ranking method with fidelity loss," in *International ACM SIGIR Conference on Research and Development in Information Retrieval*, 2007, pp. 383–390.
- [54] J. Kim, A.-D. Nguyen, S. Ahn, C. Luo, and S. Lee, "Multiple level feature-based universal blind image quality assessment model," in *IEEE International Conference on Image Processing*, 2018, pp. 291–295.
- [55] S. P. Lloyd, "Least squares quantization in PCM," *IEEE Transactions on Information Theory*, vol. 28, no. 2, pp. 129–137, Mar. 1982.

- [56] E. C. Larson and D. M. Chandler, "Most apparent distortion: Full-reference image quality assessment and the role of strategy," *Journal of Electronic Imaging*, vol. 19, no. 1, pp. 1–21, Jan. 2010.
- [57] H. Lin, V. Hosu, and D. Saupe, "KADID-10k: A large-scale artificially distorted IQA database," in *International Conference on Quality of Multimedia Experience*, 2019, pp. 1–3.
- [58] M. Perez-Ortiz, A. Mikhailiuk, E. Zerman, V. Hulusic, G. Valenzise, and R. K. Mantiuk, "From pairwise comparisons and rating to a unified quality scale," *IEEE Transactions on Image Processing*, vol. 29, pp. 1139–1151, 2020.
- [59] Z. Duanmu, W. Liu, Z. Wang, and Z. Wang, "Quantifying visual image quality: A bayesian view," *CoRR*, vol. abs/2102.00195, 2021.
- [60] K. He, X. Zhang, S. Ren, and J. Sun, "Deep residual learning for image recognition," in *IEEE Conference on Computer Vision and Pattern Recognition*, 2016, pp. 770–778.
- [61] D. Kingma and J. Ba, "Adam: A method for stochastic optimization," in *International Conference on Learning Representations*, 2015.
- [62] D. Lopez-Paz and M. Ranzato, "Gradient episodic memory for continual learning," in *Advances in Neural Information Processing Systems*, vol. 30, 2017, pp. 6467–6476.
- [63] D. Rolnick, A. Ahuja, J. Schwarz, T. P. Lillicrap, and G. Wayne, "Experience replay for continual learning," in *Advances in Neural Information Processing Systems*, vol. 32, 2019, pp. 350–360.